A Dynamic Light Scattering Study of Four DNA Restriction Fragments

Susan S. Sorlie and R. Pecora*

Department of Chemistry, Stanford University, Stanford, California 94305.
Received May 23, 1989; Revised Manuscript Received July 17, 1989

ABSTRACT: Dynamic light scattering time correlation functions from dilute solutions of linear, monodisperse DNA restriction fragments, ranging in size from 367 to 2311 base pairs (molecular weight from 0.24 to 1.5 million), were measured at 20 °C, in 100 mM NaCl, 10 mM Tris·HCl, and 1 mM EDTA (pH 8). The correlation functions were analyzed by using CONTIN, a constrained inverse Laplace transform program. At scattering angles of 16 and 22°, the correlation functions are consistent with single exponential decays representing the translational motion of the DNAs. At higher angles, the correlation functions generally exhibit two or more relaxation modes reflecting the internal dynamics in addition to the translational diffusion of the DNAs. The distribution of relaxation times is consistent with theoretical simulations based on the Rouse–Zimm free draining model for a flexible coil with experimental input parameters for the radius of gyration and translational diffusion coefficient. The translational diffusion coefficients are predicted well by the Yamakawa and Fujii theory for the dynamics of wormlike chains. The diffusion coefficients vary with the molecular weights to the 0.68 power. The rotational or first internal decay time is consistent with the Rouse–Zimm model in the free draining limit. The persistence length from a comparison of experimental diffusion coefficients with the predicted diffusion coefficients based on the theories of Yamakawa and Fujii, Yamakawa and Yoshizaki, or Hagerman and Zimm does not show a clear dependence on the contour length of the DNAs. The general results are consistent with transient electric birefringence experiments performed previously on the same fragments.

I. Introduction

The dynamics of single macromolecules in dilute solution is one of the classic problems in polymer physics. The object of such studies is to obtain a fundamental understanding of the translational, rotational, and long-range intramolecular dynamics of macromolecules with degrees of stiffness ranging from rigid rods to flexible coils. Much work, both experimental and theoretical, has been done on the limiting cases of very flexible coils and on rigid rods (usually virus particles such as tobacco mosaic virus). For semistiff rodlike macromolecules both the experimental and theoretical techniques for studying the dynamics are still largely undeveloped, despite the great importance of such molecules in both biological and materials applications. In this paper, we extend and adapt the polarized dynamic light scattering technique and use it to study the dynamics of a homologous series of monodisperse semistiff rodlike macromolecules in dilute solution.

The polarized dynamic light scattering experiment (DLS), unlike some other techniques such as electric birefringence and viscoelastic dispersion and relaxation, allows for a "nonperturbing" observation of the dynamics of semistiff macromolecules in dilute solution. In principle, DLS allows for the observation of translational, rotational, and long-range internal motions, via a distribution function of relaxation times. A number of difficulties have, however, inhibited the observation of rotational and long-range internal motions. Often the relaxation times for these internal modes are closely spaced together and resolution of the individual relaxation times is extremely difficult. Effects of polydispersity of the macromolecule and the inevitable small amounts of "dust" present in the solution tend to smear these relaxation decay times together. In addition to these data analysis problems, there are no adequate theoretical treatments of the dynamics of semistiff macromolecules that predict polarized DLS time correlation functions from which a distribution of relaxation times may be obtained and can be compared with the experimental distribution of relaxation times. A reliable model independent method of data analysis is necessary. Experiments that seek to provide the basis for fundamental theories should be performed on well-characterized, monodisperse macromolecules, preferably on a homologous series.

DNA restriction fragments can serve as a useful model systems for semistiff macromolecules in solution. The results of experiments on them provide a data base that may be used to test dynamical theories of semistiff molecules and to obtain information on parameters appearing in such theories. A homologous series of four linear DNA restriction fragments is used in this paper as a model system for semistiff macromolecules. These fragments have been obtained through genetic engineering techniques[1] and were constructed to exhibit a range of flexibilities in the semistiff regime. They were designed to be relatively easy to make in sufficient quantities to perform dynamic light scattering measurements on them. They meet the requirements of being both mondisperse and well characterized.

CONTIN[2-5] is a sophisticated, model independent data analysis program that inverts the time correlation function obtained from DLS experiments to give a distribution of relaxation times. No assumptions need be made about molecular scattering form factors. It is rapidly becoming the "standard" data analysis method for DLS experiments because it extracts the maximum amount of information from the data without overinterpreting the data. Many of the time correlation functions obtained from DLS experiments on the DNA restriction fragments are composed of a complex combination of decay processes due to the large number of long-range internal motions occurring in solution. Many of these internal motions decay on nearly the same time scale, so that the separate relaxation times cannot be resolved. The use of CONTIN in this case is especially important because it allows for broad peaks in the distribution function due to a complex set of decay processes. In this paper, CONTIN has been systematically applied to the analysis of DLS

0024-9297/90/2223-0487$02.50/0

experiments from the DNA restriction fragments.

The theoretical problem of the dynamics of semistiff macromolecules in dilute solution has not yet been satisfactorily resolved because of the multiplicity of difficult to treat contributions to the dynamics. Semistiff macromolecules exhibit restoring forces to bending, hydrodynamic interactions between different segments of the chain, excluded volume forces between distant parts of the chain, and for molecules such as the DNAs, polyelectrolyte effects. Theories that incorporate some of these effects have been formulated, although none of these theories incorporate all of them in a consistent manner. Often within each theory of large number of parameters are floated or the equations are mathematically complex. This makes it difficult to calculate the form of the distribution of decay times for the internal motions. Thus, for theories that incorporate realistic effects, such as stiffness, a direct comparison with the distribution of decay times obtained from dynamic light scattering is very difficult.

The free-draining Rouse–Zimm model is a simple model that does not directly incorporate stiffness, excluded volume effects, or hydrodynamic interactions between the segments. However, because of its mathematical simplicity, the time correlation function from dynamic light scattering can be easily predicted for this model. In this paper, theoretical comparisons to experiment have been made by using the free-draining Rouse–Zimm model. The effects of hydrodynamic interactions, stiffness, and excluded volume are indirectly incorporated by using experimental input parameters that contain some of these effects. This method lacks physical rigor, however, it can serve as a useful guide to the interpretation of actual experimental data by computing theoretical DLS time correlation functions and then applying CONTIN analysis to them.[6] Brownian dynamics simulations[7] have also been utilized (although only to a limited extent) for comparing dynamical models with the results of the DLS experiments. This method is very powerful and can include both effects of stiffness and hydrodynamic interactions (both preaveraged or non preaveraged). These theoretically generated distributions show how peaks in measured relaxation time distributions may be merged together. The models are, thus, particularly useful as a guide to the analysis of DLS data for information on internal motions, especially for the largest DNA fragment studies where several unresolved internal modes contribute at high scattering angles. A detailed discussion of the application of this method to the study of a 2311-bp DNA fragment has been given previously.[6] This paper is hereafter referred to as I.

The homologous series of four DNA restriction fragments has a range of flexibilities from semistiff to flexible coil. The longest is the 2311-bp fragment, approximately 16 persistence lengths in contour length. In I, it was found that the dynamical behavior of this fragment closely follows predictions of the Rouse–Zimm model in the free-draining limit with experimental input parameters for the radius of gyration and the translational diffusion coefficient. The 1010-bp fragment is approximately seven persistence lengths. It might be expected to exhibit behavior with a larger effect due to stiffness. The 762-bp fragment is five persistence lengths long. The 367-bp fragment is the smallest and stiffest fragment and contains 2.5 persistence lengths. It should exhibit the most rodlike behavior. To examine the apparent amount of flexibility exhibited by each fragment, the relaxation time distribution functions from CONTIN were obtained. These are compared with theoretical distribution functions in the rod and coil limits. Values of the translational diffusion and rotational (internal decay) coefficients were obtained from the experimental distribution functions and compared with theory. How these variables change with size is studied. In this way conclusions can be drawn about how the flexibility of the DNA affects its dynamics.

II. Methods

Sample Preparation. Dilute solutions of the three smaller DNA restriction fragments were prepared for dynamic light scattering experiments. (The preparation of the 2311-bp fragment is described in I.) The lengths of these fragments were 1010, 762, and 367 bp. The plasmids pLH1010 and pLH762/367, from which these fragments were obtained were constructed from pBR322 in our laboratory.[1] pLH1010 is a 6383-bp plasmid containing two identical copies of the 1010-bp fragment. The pLH762/367 is 7132 bp long and contains three identical copies of the 762-bp fragment. The 367-bp fragment (which is actually a combination of a 367- and 368-bp fragment) was obtained from further digestion of the 762-bp fragment. Each plasmid was used to transform *E. coli* strain HB101 from which it was purified using a slightly modified method of Marko, Chipperfield, and Birnboim.[8] The plasmids were then digested with PvuII from New England Biolabs in MSB (50 mM NaCl, 10 mM Tris·HCl (pH 7.5), 10 mM $MgCl_2$, and 1 mM dithiothretol) for approximately 2 h to obtain the 1010- and 762-bp fragments. The resulting fragments were separated from the larger fragments and any contaminants of different size or shape by using multiple selective PEG precipitations.[9] To obtain the 367-bp fragment, some of the 762-bp fragment was further digested under the same conditions with HaeIII and selectively precipitated from the smaller fragments with PEG. The resulting DNA pellets were resuspended in TNE (100 mM NaCl, 10 mM Tris·HCl (pH 8.0)) and extracted once with phenol and once with a 50/50 mixture of phenol/chloroform. Following this, three chloroform/isoamyl alcohol (24/1) extractions and three extractions with water-saturated ether were performed. The plasmid solutions were ethanol precipitated twice and resuspended in TNE. The final concentrations used were 350 mg/mL for 367 base pair fragment, 210 mg/mL for the 762 base pair fragment, and, 190 mg/mL for the 1010 base pair fragment. The solutions were filtered through a Gelman ARCO LC13 0.2 μm pore size filter into a clean Spectrocell 10-mm square Pyrex cuvette. The solution was examined for dust through a 5× microscope during illumination with laser light. When clean, the sample was allowed to equilibrate for 20 min at 20 °C before measurements were made. All measurements were performed at 20 °C.

Sample Purity. To determine if the samples contained impurities that would interfere with the observation of rotational motion, the dynamic light scattering time correlation function was measured at low angle. At this angle only one peak in the distribution function should be observed. Any extra peaks would indicate the presence of impurities. The DLS time correlation function was then analyzed by using both CONTIN and DISCRETE. If either analysis gave more than one sharp peak in the distribution function, it was considered unsuitable. This does not include a peak at fast times (a few microseconds), which is presumed to be from after pulsing or an artifact of the data analysis program CONTIN.

It is very important to painstakingly check the purity of the DNA fragments in solution. Many methods for separating the restriction fragments are found to be unsuitable for DLS measurement. In particular, a high-yield method for removing agarose from samples that were separated by using gel electrophoresis has not been found. Some of the methods tried include DEAE paper,[1] homogenation followed by a hydroxylapatite column[10] or binding to glass powder,[11] and electrophoresis into hydroxylapatite.[12,13] Potassium iodide density gradients[14,15] work well for large DNA's, but the small size of our fragments made the bands too broad to obtain good separation. Electroelution[15] and electroelution using a unidirectional electroelutor (Analytical, manufactured by IBI, catalogue number 46000) was also tried unsuccessfully. Low melting point (LMP) agarose fol-

lowed by a phenol extraction[16] did not work. Ion-exchange and size exclusion HPLC were also tried without success. Unfortunately, the extra DLS decay time observed at low angles when agarose, or some impurity in agarose, is present in the solution is close enough to the decay time for rotational motion observed at higher angles that this impurity is not tolerable.

Multiple PEG precipitations are chosen to separate the fragments because they did not give any extra peaks in the low-angle DLS distribution function. PEG precipitation has the advantage of giving high yields (>90%), being very inexpensive and easy to prepare even in large batches. Suitable purity is also obtained when the sample from the hydroxylapatite column was run through a NACS prepac column, although the yield is not as high as desirable and only small NACS prepac columns were available. DLS measurements were performed on this sample, and the results are the same as those obtained when the sample is purified with a selective PEG precipitation. This suggests that the DLS measurements performed on samples purified by PEG precipitation are not significantly altered by the presence of a small amount of PEG remaining in solution.

After data collection, the DNA concentration was measured by UV absorption at 260-nm wavelength. The ratio of the absorbances at 260 and 280 nm was measured to check for possible contamination with protein or phenol. The DNA fragments were checked for degradation by agarose gel electrophoresis. At 20 °C, the DNA show no detectable degradation over a period of 1–2 days.

Experimental Apparatus. The light scattering apparatus used in the experiments is discussed elsewhere.[17] The laser power was between 0.2 and 1.5 W. The homodyne autocorrelation function was measured by using a Brookhaven Bi2030AT digital correlator with 136 real time data points. The first data point from each data set was not used. The scattering angles at which correlation functions were measured ranged from 16 to 128°. Typical signal to RMS noise ratios (defined as the value of the second point minus the base line all divided by the RMS fluctuation in the delay channels) are between 1000 and 2000 for the 1010-bp fragment and approximately 1000 for the smaller two fragments. The data was electronically transferred from the Brookhaven correlator to a Universe 68 microcomputer manufactured by Charles River Data systems. The square root of the data minus the base line (what is often called $g^1(\tau)$) was then analyzed by using versions of the Fortran programs CONTIN and DISCRETE. A description of these programs and their capabilities is given in I.

III. Theory

Rouse–Zimm Free-Draining Limit. This limit has been discussed in detail in paper I, and only a brief summary of the relevant equations is given here. The translational diffusion coefficient, D, depends on the friction coefficient of a bead, ζ, and the number of beads, n

$$D = k_B T/n\zeta \tag{1}$$

where k_B is Boltzmann's constant and T is the absolute temperature. A theoretical value for D cannot be calculated by using eq 1, unless the number of beads and the friction on a bead is assumed. The internal decay times, as defined by Zimm, are

$$\tau_k = R_G^2/\pi^2 D k^2 \qquad k = 1, ..., n \tag{2}$$

Rouse–Zimm Nondraining Limit. In the nondraining limit of the Rouse–Zimm model hydrodynamic interaction between different segments drives the diffusion equation. These effects are described by the Oseen interaction tensor, which is in turn derived from the Navier–Stokes equation of hydrodynamics. The Oseen interaction tensor describes how the velocity of a segment is affected by the motions of the solvent molecules due to the motion of the other segments in the chain, assumed to be point sources of motion. It depends on the reciprocal of the distance between segments and is, in this version of the model, preaveraged by assuming a Gaussian distribution of the distance between segments. The diffusion coefficient in the nondraining limit is given by

$$D = \frac{0.192 k_B T}{\eta_0 6^{1/2} R_G} \tag{3}$$

where T is the absolute temperature, η_0 is the viscosity of the solvent, and R_G is the radius of gyration. The internal decay times are

$$\tau_k = \frac{11.8\eta_0 R_G^3}{k_B T \lambda_k} \qquad k = 1, ..., n \tag{4}$$

The λ_k's have been calculated for some of the longer wavelength decay modes ($\lambda_1 = 4.04$) and are given in ref 18. The calculation of the dynamic form factor is more complex in this limiting case and has not yet been calculated.

Rouse–Zimm Intermediate Draining. In the intermediate draining limit the diffusion coefficient is the sum of two terms. The first term arises from Brownian motion while the second term arises from hydrodynamic interactions between segments

$$D = \frac{k_B T}{n\zeta}\left(1 + \frac{8}{3}X\right) \tag{5}$$

where $X = 2^{1/2}h$. The hydrodynamic interaction or draining parameter, h, is proportional to ζ and is a measure of the strength of the hydrodynamic interactions. The hydrodynamic interaction parameter can be calculated for a given experimental system. In the free-draining limit the first term dominates ($X = 0$) and in the nondraining limit the second term is dominant (X (or ζ) $\rightarrow \infty$). A true polymer probably diffuses with contributions from both terms.

In between the nondraining and free-draining limits the calculation of the dynamic form factor is mathematically complex. Perico et al.[19] have calculated the coefficients of the dynamic form factor for $n = 100$ and $h = 0$ (free-draining), $h = 1$ (contributions from the first term in eq 5 for the diffusion coefficient contributing about 40% and the second term in eq 5 contributing the rest), and $h = 2$. The $h = 0$ calculation for the dynamic form factor gives results that differ only a small amount from those calculated in the limit of the number of beads going to infinity, $n \rightarrow \infty$. Later Tsunashima et al.[20] calculated the normalized amplitude contribution from translational motion, S_0/S, for $n = 100$ and $h = 2.67$ (contributions from the first term in eq 5 for the diffusion coefficient contributing about 10% and the second term contributing the rest). The scattering amplitudes and the ratios of scattering amplitudes in the free-draining and intermediate draining cases were found to be very similar. These amplitude ratios are such that given the uncertainty in typical DLS experimental data it would be very difficult to distinguish between them. Recently, Rey, Freire, and Garcia de la Torre,[21] performed Brownian dynamics simulations of the Rouse–Zimm model on chains of 4–20 beads. They found that the scattering amplitudes and the decay times were similar to those predicted by the preaveraged, nondraining Rouse–Zimm theory.

Wormlike Chain Theories. In between the Gaussian coil and rigid-rod limits there are few theories that describe the dynamics of a macromolecule in solution. Generally these theories predict values of the translational diffusion coefficient and the rotational constant for chains of a given diameter, contour and persistence

length, but do not give the full distribution of relaxation times, including the relative amplitudes expected in a DLS experiment.

Hagerman and Zimm. Hagerman and Zimm[22] have utilized a Monte Carlo method to create an ensemble of coil configurations for a wormlike chain with hydrodynamic interactions and a small correction for the difference in position of the center of mass and the center of hydrodynamic resistance. The average rotational diffusion coefficient was calculated by assuming each configuration was a rigid body and then averaging over the ensemble. This model predicts the ratio between the rotational constant for a rigid rod as determined by Broersma[23] and that for a wormlike coil. This relationship depends on both the persistence length, P, and the contour length, L, of the wormlike coil, and, according to Hagerman and Zimm, is valid for $0.1 < L/P < 5$. Hagerman and Zimm's result is

$$\frac{\Theta_{\text{Broersma}}}{\Theta_{\text{worm}}} = R_a(1 - Y) \tag{6}$$

where

$$R_a = 1.0120 - 0.24813x + 0.033703x^2 - 0.0019177x^3$$

$$Y = 0.06469x - 0.01153x^2 + 0.0009893x^3$$

here $x = L/P$.

Yamakawa. Yamakawa and Fujii[24] evaluated the diffusion coefficient for a wormlike coil by using wormlike cylinder models without excluded volume. Hydrodynamic interactions are evaluated by using the Oseen–Burgers procedure. The diffusion coefficient is given in terms of a reduced length, $L/2P$, and a reduced diameter, $d/2P$. The equation for the diffusion coefficient is complicated, and the reader is referred to the original paper. Yoshizaki and Yamakawa[25] evaluate the rotational decay time, τ_D, for a wormlike chain by using a discrete helical wormlike chain model, and in terms of the rotational decay time for a rigid rod $\tau_{D,rod}$

$$\tau_D = \frac{\tau_D^{rod}}{(L)^3}\left[L' + \frac{1}{2}(e^{-2L'} - 1) \right]^{3/2}[1 + 0.539526 \ln (1 + L')] \tag{7}$$

where $L' = L/2P$ and $L' \leq 30$, and $\tau_{D,rod}$ is calculated by using the Broersma relation (given below) for the rotational constant, Θ, and relating that to the rotational decay time.

$$\tau_{D,rod} = 1/6\Theta \tag{8}$$

Rigid Rod. The rigid-rod model consists of a rod of length L, composed of n identical, optically isotropic segments and a diameter that is negligible compared to the wavelength of light. In this model translational and rotational motion are assumed to be independent of one another. Pecora[26] gave the dynamic structure factor for this model as a function of the contour length and the scattering vector length. The dynamic structure factor, $S(q,t)$, can be calculated by using the translational diffusion coefficient obtained from experiment and the rotational constant obtained from the Broersma relations.

Broersma Relations. The Broersma relations[23] for a long rigid rod of length L and diameter d are

$$D = \frac{k_B T}{3\pi\eta_0 L}\left[\delta - \frac{1}{2}(\gamma_{II} + \gamma) \right] \tag{9}$$

$$\Theta = \frac{3k_B T}{\pi\eta_0 L^3}(\delta - \zeta) \tag{10}$$

where

$$\delta = \ln (2L/d)$$

$$\gamma_{II} = 1.27 - 7.4(1/\delta - 0.34)^2$$

$$\gamma = 0.19 - 4.2(1/\delta - 0.39)^2$$

$$\zeta = 1.45 - 7.5(1/\delta - 0.27)^2$$

These relations are valid in the limit of a long contour length with respect to diameter, $L/d > 4$.

IV. Results and Discussion

The CONTIN distribution of relaxation decay times (given in terms of an effective hydrodynamic radius, R_h) gives at most two peaks clearly attributable to DNA dynamics for the three smaller fragments. The peak at the largest R_h is attributed to translational motion. The second peak is attributed to both translation and first internal mode and/or rotational relaxation. Higher order internal modes are shown later to be of negligible importance in these distribution functions at the scattering angles studied. The translational contribution can be separated out of the second largest peak in the distribution function. This leaves the contribution from the first internal mode/rotational decay time.

It is unclear what kind of internal motion gives rise to this first internal mode/rotational decay time. For wormlike macromolecules, theoretical calculations are for an end-over-end rotational motion, and for Gaussian coils, which do not contain an extended axis of rotation, the first internal decay time is attributed to a long-range internal "breathing" mode. The four DNA restriction fragments are wormlike macromolecules whose first internal mode is probably neither pure rotation nor an internal breathing mode but is a rotational motion coupled with a breathing motion. For this reason we continue to refer to this relaxation time as a "first internal mode/rotational" decay time.

The peak positions and their amplitudes for the 1010- and 762-bp fragments are given in Tables I and II. Table I shows average values from both CONTIN and DISCRETE for several data sets at each angle, while Table II shows some results from just one of several data sets obtained. For the 367-bp fragment only one significant peak was observed at all scattering angles. The data are compared below with the diffusion coefficient and first internal mode/rotational decay times for the largest fragment, 2311 bp, given in I and with each other. They are also compared with the predictions of the theories mentioned in the previous section. A comparison is made between the CONTIN distribution function from our experiments and those simulated from the Rouse–Zimm model in the free-draining limit and the rigid rod.

Input parameters for the Rouse–Zimm model in the free-draining limit are the radius of gyration, R_G, which determines the amplitude of each relaxation decay time, and the translational diffusion coefficient, D, which with R_G, determines the relaxation decay times. The relaxation decay times, τ_k, are those defined by Zimm[27] in eq 2. The translational diffusion constant is obtained from low-angle DLS experiments where single exponential behavior is exhibited. The radius of gyration is calcu-

Table I
Average Peak Positions and Their Amplitudes from the CONTIN Distribution Functions and from DISCRETE for the 1010-bp Fragment

angle, deg	CONTIN and DISCRETE peak no.	size, Å	% amp
16.4	1	300 ± 7.8	100
33.0	1	298 ± 1.5	98.2
	2	14.5 ± 2.0	1.8
57.0	1	285 ± 0	95.3 ± 2.9
	2	53 ± 5.5	2.4 ± 0.1
	3	11.5 ● 0.3	2.4
73.0	1	268 ± 7.4	94.2 ± 1.4
	2	38 ± 7.7	3.9 ± 5.5
	3	9 ± 1.0	2.3
90.0	1	272 ± 6.6	90.7 ± 2.0
	2	64 ± 7.0	6.2 ± 1.7
	3	12 ± 3.4	3.1
106.4	1	273 ± 5.0	85.5 ± 1.4
	2	67 ± 9.5	10.1 ± 1.2
	2	9 ± 3.1	4.4
128.7	1	258 ± 12.2	81.7 ± 1.9
	2	74 ± 15.1	12.6 ± 2.8
	3	9 ± 3.4	5.7

Table II
Peak Positions and Their Amplitudes from the CONTIN Distribution Functions and from DISCRETE for the 762-bp Fragment

angle, deg	peak no.	CONTIN size, Å	CONTIN % amp	DISCRETE size, Å	DISCRETE % amp
21.9	1	236 ± 2	100	237	100
51.3	1	232	93.8	232	95
	2	6	6.2	7	5
(under smoothed soln)	1	233	92.8		
	2	15	0.8		
	3	5	6.4		
73.6	1	235	94.1	235	95.6
	2	22	2.8	18	4.4
	3	6	3.1		
90.0	1	228	92.1	229	89.0
	2	29	2.8	31	4.2
	3	6	5.1	4	6.8
106.4	1	229	89.7	230	87.2
	2	43	4.3	39	5.6
	3	6	6.0	4	7.2
111.9	1	222	84.8	233	76.0
	2	33	4.2	44	6.3
	3	5	11.0	4	17.7
123.0	1	243	82.4	237	69.3
	2	63	9.7	48	7.3
	3	7	7.9	3	23.4

lated from the persistence length, P, and the contour length, L, for a wormlike chain.

$$R_G^2 = P^2\left\{\frac{L}{3P} - 1 + \frac{2P}{L} - \frac{[1-\exp(-L/P)]}{(L/P)^2}\right\} \quad (11)$$

In the nondraining limit the complete correlation function has not been calculated. However the diffusion coefficient and the internal decay times can be calculated from the radius of gyration by using equations 3 and 4. R_G has been calculated by using eq 11 for a wormlike coil. Thus, with use of this R_G some effects of stiffness are incorporated into the Rouse–Zimm model.

For the wormlike chain theories, the parameters used are generally the contour length, the persistence length, and the diameter. The contour length is listed in Table III. A persistence length[28] of 500 Å and a diameter[29] of 26 Å are obtained from the literature. Small variations in the diameter are not significant for the relatively long DNA fragments used here. The effect of varying the persistence length is discussed later in this section.

Table III
DNA Restriction Parameters

DNA fragment (bp)	mol wt[a] (10^6 daltons)	L,[b] Å	R_G,[c] Å	concn, μg/mL
2311	1.50	7857	1044	...
1010	0.67	3434	620	190
762	0.50	2591	510	210
367	0.24	1248	291	350

[a] Based on 660 daltons/bp. [b] Based on 3.4 Å/bp. [c] The radius of gyration was calculated by using eq 11.

Table IV
Diffusion Coefficients[a]

DNA sample	10^8D, cm²/s: 2311 (L/P = 16)	1010 (L/P = 7)	762 (L/P = 5)	367 (L/P = 2.5)
experimental	4.56 ± 0.13	7.15 ± 0.19	9.05 ± 0.11	15.8 ± 0.47
Rouse–Zimm (nondraining)	3.04	5.11	6.21	10.9
Yamakawa and Fujii	4.31	7.59	9.27	15.7
Broersma	3.23	6.29	7.84	13.2

[a] $R_h = 2.145 \times 10^{-13}/D$.

Parameters for the rigid-rod model are the contour length for determining the amplitude of the relaxation times and L and d for determining the translational and rotational diffusion coefficients. For the simulated distribution functions the translational diffusion coefficient was obtained from experiment and the rotational diffusion coefficient was calculated from the Broersma relations given in equations 9 and 10. The experimental translational diffusion coefficient was used instead of the prediction from the Broersma relations because it gave better agreement with the experimental data.

Table III gives the parameters that vary with molecular weight. The concentration of the DNA solutions is also given for the three shorter fragments.

Translational Diffusion Constants. The translational diffusion coefficient has been calculated from the decay time, τ, obtained from low-angle and low-concentration DLS experiments, through the relation

$$D = 1/\tau q^2 \quad (12)$$

where q is the scattering vector length. Table IV gives the diffusion coefficients for each DNA fragment.

First Internal/Rotational Decay Time. At higher scattering angles in the DLS experiment, two significant peaks are often obtained from both CONTIN and DISCRETE; as stated previously the first peak was assumed to be from translational motion and the second peak was from translation and the first internal/rotational decay time. The first internal/rotational decay time, τ, is calculated both from the smaller peak in the CONTIN distribution function (which corresponds to a faster decay time, τ') and from the faster decay time, τ', in the DISCRETE analysis. In both cases the inverse decay time, q^2D, from translational motion was subtracted out by using the following equation

$$\tau = (1/\tau' - q^2D)^{-1} \quad (13)$$

Here q is the scattering vector length and D is the translational diffusion coefficient. The results are given in Table V.

To determine if the higher order internal modes were negligible, the first internal/rotational decay time is plotted as a function of the scattering angle and is shown in Figure 1. Figure 1 (top) is for the 762-bp fragment while Figure 1 (bottom) is for the 1010-bp fragment. In both plots the first internal/rotational decay time is indepen-

Table V
"First Internal/Rotational" Decay Times

DNA sample	τ_1, μs 2311 (L/P = 16)	1010 (L/P = 7)	762 (L/P = 5)
experimental	266[b]	56.5 ± 14.4	26.0 ± 6.6
Rouse–Zimm (free draining)	242	54.5	29.1
Rouse–Zimm (nondraining)	822	172	95.8
Hagerman and Zimm[a]		89.9	58.8
Yamakawa andYoshizaki[a]	448	93.4	56.8
Broersma[a]	5000	417	193

[a] $\Theta \equiv 1/6\tau_1$. [b] From data obtained at a single scattering angle.[6]

dent of the scattering angle to within the scatter in the data. If the first internal/rotational decay time did contain contributions from higher internal modes, then it would decrease with scattering angle, as faster modes contribute more significantly.

The first internal/rotational decay time for the 2311-bp fragment is given in Table V. For this fragment higher order internal modes contribute to the time correlation function at the higher angles, and there is only a small range of angles where higher order terms can be assumed to be negligible. Thus, the value for this fragment was obtained from data obtained at a single angle (see I). The value of the first internal/rotational decay time given here is a factor of 2 smaller than was reported in I because of a difference in definition. In contrast to Zimm's analysis (see eq 2) used here, in Pecora's analysis (see Berne and Pecora,[30] eq 8.8.14,) the $1/\tau'$ in eq 13 is replaced by a $2/\tau'$ (eq 14 of I). As emphasized previously, this difference does not have any physical significance and, although it is a source of much confusion in the literature, is simply a matter of definition. The first two significant terms in the expansion of k in the dynamic form factor (eq 3 of I) have the same decay times. In Zimm's analysis the first decay time is the sum of these two decay times while in Pecora's analysis the first internal decay time is equal to one of these decay times or half that from Zimm's analysis.

Comparison with Theories. For the 367-bp DNA fragment the ratio of the contour length to the persistence length is estimated to be L/P = 2.5. This fragment shows the least flexibility and should exhibit behavior most similar to that of the rigid rod. The translational diffusion coefficient for the 367-bp fragment is (15.8 ± 0.47) × 10^{-8} cm^2/s. The value for the first internal/rotational decay time could not be determined in the q range accessible in the DLS experiment by using laser light of wavelength of 488 nm. Yamakawa and Fujii's model gave the best agreement with the experimental diffusion coefficient. Their model predicts a value of 15.7 × 10^{-8} cm^2/s. The Broersma prediction for the translational diffusion coefficient gives closer agreement with experiment than does the Rouse–Zimm model in the nondraining limit. See Tables IV and V.

For the 762-bp fragment the ratio of the contour length to the persistence length is approximately L/P = 5.0. The translational diffusion constants calculated from Yamakawa and Fujii's model (9.27 × 10^{-8} cm^2/s) agrees well with the experimental value ((9.05 ± 0.11) × 10^{-8} cm^2/s.) The value from the Broersma relation (7.84 × 10^{-8} cm^2/s) gives, within the experimental error, about the same percentage error as for the 367-bp fragment. Again the value for the translational diffusion coefficient predicted by the Rouse–Zimm model in the nondraining limit is not in particularly good agreement with experiment. The experimental value for the first internal/rotational decay time is 26 μs. The Rouse–Zimm model in the free-draining limit gives the best agreement with the first internal/rotational decay time. The value predicted is 29.1 μs. The predictions from Yamakawa and Yoshizaki, Hagerman and Zimm, Broersma, and Rouse–Zimm in the nondraining limit do not agree particularly well with the experimental value.

For the 1010-bp fragment, L/P = 7. The experimental value of the diffusion coefficient is (7.15 ± 0.19) × 10^{-8} cm^2/s, which is in good agreement with the theoretical predictions from the Yamakawa and Fujii model (7.59 × 10^{-8} cm^2/s.) The Rouse–Zimm model in the nondraining limit does not agree with the experimental value. For the first internal/rotational decay time the experimental value (56.5 μs) again agrees quite well with the Rouse–Zimm value (54.5 μs) in the free-draining limit. Hagerman and Zimm's value (8.9 μs) and Yamakawa and Yoshizaki's value (93.4 μs) are not close.

For the 2311-bp fragment, L/P = 15. The experimental diffusion coefficient obtained ((4.56 ± 0.13) × 10^{-8} cm^2/s) is in good agreement with the prediction of the Yamakawa and Fujii model (4.31 × 10^{-8} cm^2/s). The other models do not predict the value of the diffusion coefficient very well. It was shown in I that the internal dynamics of this fragment are in close agreement with that predicted by the Rouse–Zimm model in the free-draining limit (using experimental values for D and R_G). The first internal/rotational decay time from experiment (266 μs) is in close agreement with the predicted value (242 μs) for the Rouse–Zimm model in the free-draining limit. As expected, for a fragment this flexible, the agreement with the other models is not very good.

The free-draining Rouse–Zimm model, with input parameters that contain effects due to the stiffness of the DNA fragment, does not make predictions for the value of the diffusion coefficient. It, however, does a very good job of predicting the first internal/rotational decay times for the DNA fragments. The Rouse–Zimm model in the nondraining limit does not seem to predict any of the values particularly well. It does best for the diffusion coefficients (error about 30%). Hagerman and Zimm's model makes predictions for L/P ratios less than 5. It should only apply to the first internal/rotational decay time for the 367-bp fragment (for which the first internal/rotational decay time was not obtained.) However, it does predict the value for the 1010-bp fragment well. The values for the diffusion coefficient predicted by Broersma are within 12–17% of the experimental values for the three smaller fragments but are off by almost 30% for the 2311-bp fragment. The rotational decay times predicted by Broersma are not close to the experimental first internal/rotational decay times for any of the fragments. (Recall, however, that a second decay time was not measured for the 367-bp fragment.) The Yamakawa and Fujii model predicts the values of the diffusion coefficient well for all the fragments. The Yamakawa and Yoshizaki model does not predict values for the first internal/rotational decay time that agree with the experimental values. In summary, Yamakawa and Fujii's model for translational motion agrees best with our experiments, and the Rouse–Zimm model in the free-draining limit gives the best predictions for the first internal/rotational decay time.

Molecular Weight Dependence of the Translational Diffusion Coefficient. The molecular weight dependence of the diffusion coefficient is given in Figure 2. The length of the corresponding fragment in base pairs is given in parentheses for each point. The power dependence of the molecular weight is obtained from the

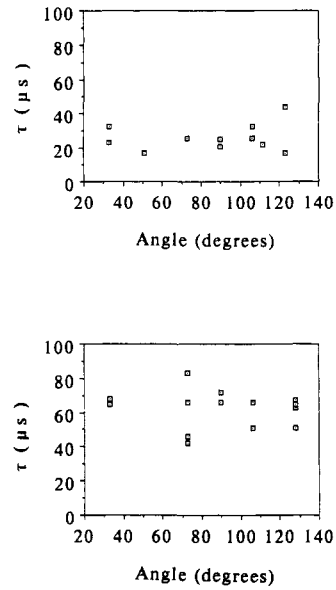

Figure 1. The first internal decay time as a function of scattering angle. The first internal decay time from the CONTIN analysis is plotted as a function of scattering angle for the 762-bp (top) and the 1010-bp (bottom) DNA restriction fragments.

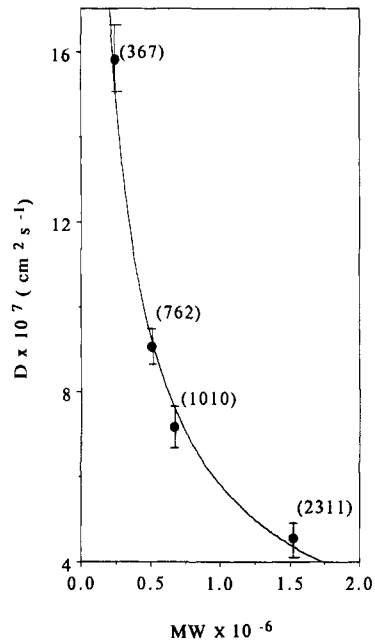

Figure 2. The molecular weight dependence of the translational diffusion coefficient. A plot of the diffusion coefficient versus the molecular weight including a least-squares fit to the experimental points (solid line).

slope of a linear least squares fit to a double logarithmic plot of the data (Figure 3). The diffusion coefficient shows a −0.68 order power dependence on the molecular weight. Both the rigid-rod and the Rouse–Zimm model in the free-draining limit predict a power dependence of −1. The Rouse–Zimm model in the nondraining limit predicts a dependence of −0.5. This increases to −0.6 with excluded volume effects included. When the radius of gyration from eq 11 is used in the nondraining Rouse–Zimm model and for Yamakawa and Fujii's model, a simple power dependence to the molecular weight is not predicted. In these two cases, the log of both the molecular weights and the diffusion coefficient predicted for each DNA fragment are plotted and fit to a straight line. Figure 3 gives log–log plots of the molecular weight dependence of D for the theories of Yamakawa and Fujii and the nondraining Rouse–Zimm model (R_G from eq 11). The experimental data is also given for comparison. A least-squares fit to the data is also shown for all three cases. The power dependence of the diffusion coefficient on the molecular weight for the nondraining Rouse–Zimm model is −0.69 when stiffness is added by using the radius of gyration from eq 11. Yamakawa and Fujii's model for the semistiff chain predicts a power dependence of −0.70.

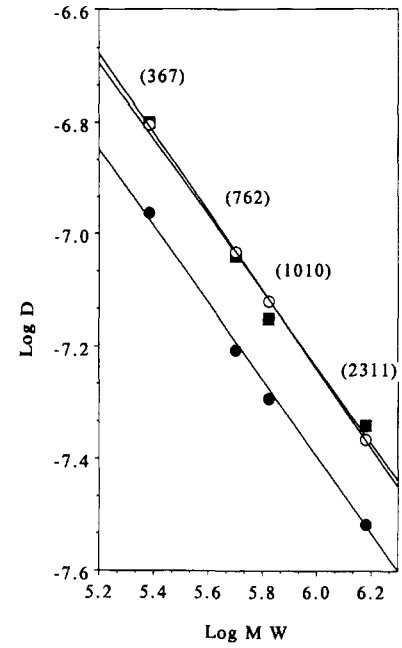

Figure 3. log–log plot of the experimental data from Figure 2 with a linear fit to the points (open circles) as well as points calculated from the Yamakawa–Fujii theory (squares) and the nondraining Rouse–Zimm theory (filled circles) with linear fits to the theoretical points.

The actual dependence of the diffusion coefficient on molecular weight is probably not a simple power dependence. The dependence observed could also be explained by the fact that the smaller fragments are more rodlike, while the longer fragments are more coillike. Rodlike fragments have a power dependence closer to −1 and the coillike fragments have a dependence closer to a coil with contributions from hydrodynamic interactions and possibly excluded volume effects.

The Dependence of the Diffusion Coefficient and the First Internal/Rotational Decay Time on the Persistence Length. Hagerman[31] has suggested that the persistence length may be reduced by electrostatic end effects for short DNA fragments. For the three shortest DNA fragments, Lewis, Pecora, and Eden[29] have found that, decreasing the persistence length with decreasing contour length, for the most part, provides better agreement between their transient electric birefringence data and the theoretical predictions of Hagerman and Zimm. In this comparison, they identified the slowest decay time in their TEB decay with the rotational constant from theory

$$\tau = 1/6\Theta \qquad (14)$$

A persistence length of 1000 Å is generally given for DNA fragments at the low salt concentrations usually used in the TEB experiments. Their results show that for the 1010-bp fragment, a persistence length of 1000 Å gives the best agreement between experiment and theory. The 762-bp fragment requires a persistence length of 700 Å, and for the 367-bp fragment, a persistence length

Table VI
Rotational Decay Times from TEB Experiment and Theoretical Decay Times at Several Persistence Lengths

DNA length, bp	rotational decay times, μs: obsd	Rouse–Zimm[a]	predicted, Hagerman and Zimm[c]: P = 500 Å	P = 700 Å	P = 1000 Å
2311	688	822		660[b]	974[b]
1010	171	172		134	175
762	78	96	59.2	77.0	97.0
367	14.4	18	13.9	16.5	

[a] Calculated by using equations 4 and 11 (P = 500 Å). [b] Numbers predicted by the theory of Yoshizaki and Yamakawa. These values are approximately equal to those predicted by Hagerman and Zimm. [c] From Lewis et al.[29]

Table VII
Rotational Decay Times from DLS Experiment and Theoretical Decay Times from Yoshizaki and Yamakawa at Several Persistence Lengths

DNA length, bp	rotational decay times, μs: obsd	predicted: P = 250 Å	P = 300 Å	P = 325 Å	P = 350 Å
2311	266		241	267	292
1010	57		53.8	58.9	64
762	26	27.9	34.0	77.0	

Table VIII
Translational Diffusion Coefficient from DLS Experiment and the Theory of Yamakawa and Fujii at Several Persistence Lengths

DNA length, bp	10^8D, cm²/s: obsd	predicted: P = 450 Å	P = 500 Å	P = 550 Å	P = 600 Å
2311	4.56	4.46	4.31		
1010	7.15		7.59	7.38	7.20
762	9.05		9.27	9.03	8.81
367	15.8		15.7		

of 500 Å gives the best agreement. The 2311-bp fragment requires a persistence length of 700 Å. These results are summarized in Table VI.

Lewis, Allison, Eden, and Pecora[32] performed Brownian dynamics simulations of the depolarized dynamic light scattering time correlation function based on a wormlike coil, for the 367-bp DNA restriction fragment. From the Brownian dynamics simulations,[32] they found that the slowest or first internal decay times are predicted to be 9.54, 14.4, and 15.5 μs based on persistence lengths of 400, 600, and 900 Å, respectively. The corresponding Hagerman and Zimm first internal decay times are 12.4, 15.7, and 17.8 μs. Thus the Hagerman and Zimm decay times are slower than the Brownian dynamics decay times.

The DLS first internal/rotational decay times for the DNA fragments in high salt solutions are listed in Table VII. Both the experimental values and the predicted values from Yamakawa and Yoshizaki are given for several persistence lengths. A persistence length of 500 Å has been experimentally obtained for the 2311-bp fragment from static light scattering measurements.[33] The persistence length necessary to obtain agreement between experiment and the Yamakawa and Yoshizaki theory decreases with decreasing size. For the 2311- and 1010-bp fragments the persistence length is 325 Å and a value slightly under that value, respectively. For the 762-bp fragment it is 250 Å. These results are consistent with the trend in the TEB results. Similar predictions are obtained by using the theory of Hagerman and Zimm.

Table VIII lists the experimental translational diffusion coefficient and the Yamakawa and Fujii prediction of the translational diffusion coefficient for several values of the persistence length. The experimental diffusion coefficient agrees with the Yamakawa and Fujii prediction for a persistence length of approximately 500 Å for the smallest fragment. For the 762-bp fragment it is 550 Å. It increases to 600 Å for the 1010-bp fragment and then drops below 450 Å for the 2311-bp fragment. The trend is consistent with what is observed for the first internal/rotational decay time although the magnitude of the change is smaller and values of the predicted persistence length are larger. The smaller range of change can be explained by the fact that translational motion is less sensitive to changes in length than rotational motion because the translational diffusion coefficient depends on the inverse length, while the rotational constant depends on the third power of the inverse contour length.

The question of interest is whether this apparent decrease in persistence length with decreasing contour length is the result of electrostatic end effects as suggested by Hagerman or because of inherent problems with the wormlike coil models of Hagerman and Zimm and Yamakawa and Yoshizaki. In the later case, both of these theories compute an average end-over-end rotational time by using a rigid ensemble of shapes. These shapes are calculated from models based on the persistence length. Brownian dynamics simulations compute averages by using a dynamic ensemble of shapes based on a given persistence length.

Both the TEB and DLS results suggest that the persistence length is not simply changing with the size of the DNA fragment because the apparent persistence length necessary to give agreement between theory and experiment seems to consistently increase with increasing size for the smallest three DNA fragments and then is radically decreased for the largest fragment. Also the value of the persistence length necessary to obtain agreement between experiment and theory for the rotational decay time and the translational diffusion coefficient for a particular fragment is very different.

It seems likely that the apparent variation in persistence length is due to inherent problems with the wormlike coil models. This could be because these theories calculate averages based on a rigid ensemble of shapes instead of a dynamic ensemble of shapes and/or they calculate a decay time based on pure rotation and exclude the possibility of rotational motion being coupled with internal breathing modes. It is probably a combination of these possibilities. For the smallest fragment, Brownian dyanamics simulations, which predict a rotational decay time based on an dynamic ensemble of shapes, seem to give values of the decay time based on a larger, more realistic value for the persistence length.[32]

R_h and R_G Relation. The ratio of R_G to R_h is found to be 2.15 ± 0.06. R_G is given by eq 11, and R_h is the experimental value. The ratio is predicted by Flory, using the Kirkwood and Riseman theory for flexible coils with full hydrodynamic interactions, to be 1.51.[34]

The First Internal/Rotational Decay Time and the Hydrodynamic Radius. The first internal/rotational decay time, τ, is related to the hydrodynamic radius, R_h, through the relation

$$\frac{1}{\tau} = \frac{K(k_B T)}{\eta_0 R_h^3} \tag{15}$$

where K is a constant. This relationship is based on predictions from the Rouse–Zimm model. The inverse of the experimental first internal/rotational decay time is plotted as a function of the inverse of the cube of the

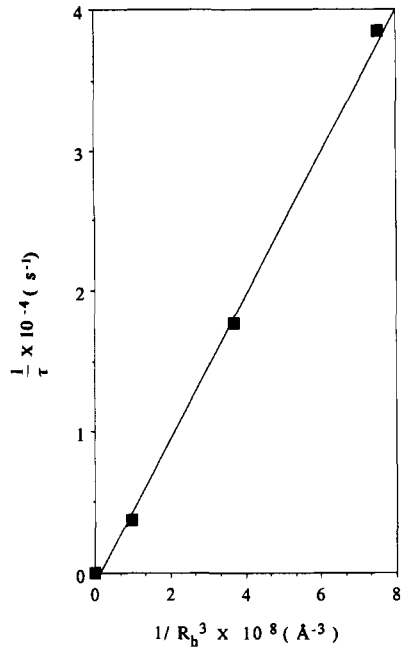

Figure 4. The first internal decay time as a function of the hydrodynamic radius.

hydrodynamic radius in Figure 4. (In Figure 4 a point has been added at the origin to bias the fit toward a zero intercept at the origin. Addition of this point, however, does not appreciably change the slope of the best fit straight line to the data points.) The slope is related to the constant K in eq 15. The experimental value of the constant K is 0.128. This constant K can be predicted both theoretically and semitheoretically. Equations 2 and 4 give the theoretical predictions for the internal decay times for the Rouse–Zimm model in the free-draining and nondraining limits, respectively. These equations depend on the radius of gyration and in the free-draining limit on the diffusion coefficient or hydrodynamic radius also. With use of the experimental relationship between the radius of gyration and the hydrodynamic radius and eq 2 or eq 4, K can be calculated semitheoretically, yielding a value of 0.113 in the free-draining limit and a value of 0.034 in the nondraining limit. With use of Flory's theoretical prediction based on the nondraining Rouse–Zimm model for the ratio of R_G to R_h given above, a completely theoretical value of K is predicted to be 0.10. A completely theoretical prediction for K in the free-draining limit is not available since in this limit no prediction is made for D. In summary, good agreement is obtained when a completely theoretical K is calculated by using the Rouse–Zimm model in the nondraining limit. However with use of the experimental ratio of R_G and R_h and the nondraining Rouse–Zimm prediction for the τ_k's (eq 4) to calculate K does not give a value for K in agreement with the experimental value. When the experimental ratio is used, the best agreement is obtained by using the free-draining Rouse–Zimm prediction for the τ_k's (eq 2).

Distribution Functions. The decay times and their corresponding amplitudes for a particular value of qR_G or qL can be calculated for the Rouse–Zimm Gaussian coil in the free-draining limit and for the rigid-rod model. The decay times and their amplitudes are used to "simulate" the correlation functions expected for these two models. The correlation functions obtained are analyzed by CONTIN, and the resulting distribution functions can be compared with the experimental distribution functions for each fragment. Figures 5–7 show the distribution function from CONTIN. The distribution functions given are from experiment, from theoretical calculations in the Gaussian coil limit, and in the rigid-rod limit. The percent of the total amplitude of each peak is given in parentheses to the right of each peak. The value of the first moment (given in terms of apparent hydrodynamic radius) for the position of several peaks is given on the abscissa directly below. The positions of the peaks and their amplitudes are summarized in Table IX. Figure 5 gives the distribution functions for the 1010-bp fragment at 90°. The experimental distribution of relaxation times contains a small peak (2.8%) at the small end of the window. It is probably due to afterpulsing or is some artifact of the data analysis program CONTIN (see I). The experimental distribution function agrees well with the distribution function predicted in the free-draining Gaussian coil limit. Figure 6 shows the distribution functions for the 762-bp fragment at 123°. The experimental distribution function agrees well with the Rouse–Zimm model in the free-draining limit. The distribution function for the 367-bp fragment at 129° is given in Figure 7 and again shows good agreement with the

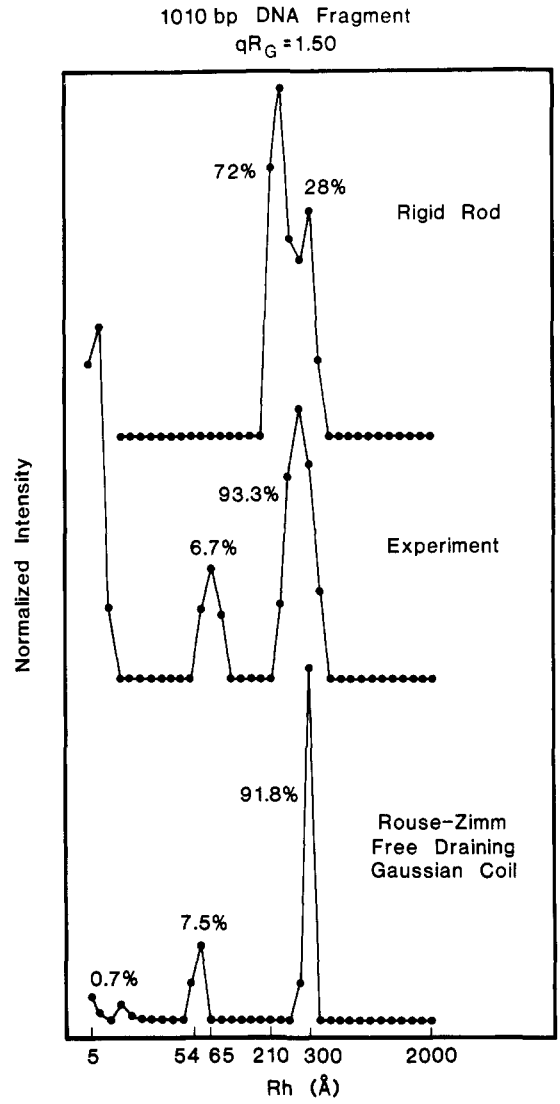

Figure 5. The CONTIN distribution function from theory and experiment for the 1010 DNA fragment. The CONTIN distribution function is given for the rigid-rod and Rouse–Zimm free-draining Gaussian coil limits and for the experimental data. The rigid-rod and free-draining Gaussian coil simulations use experimental values of the translational diffusion coefficient.

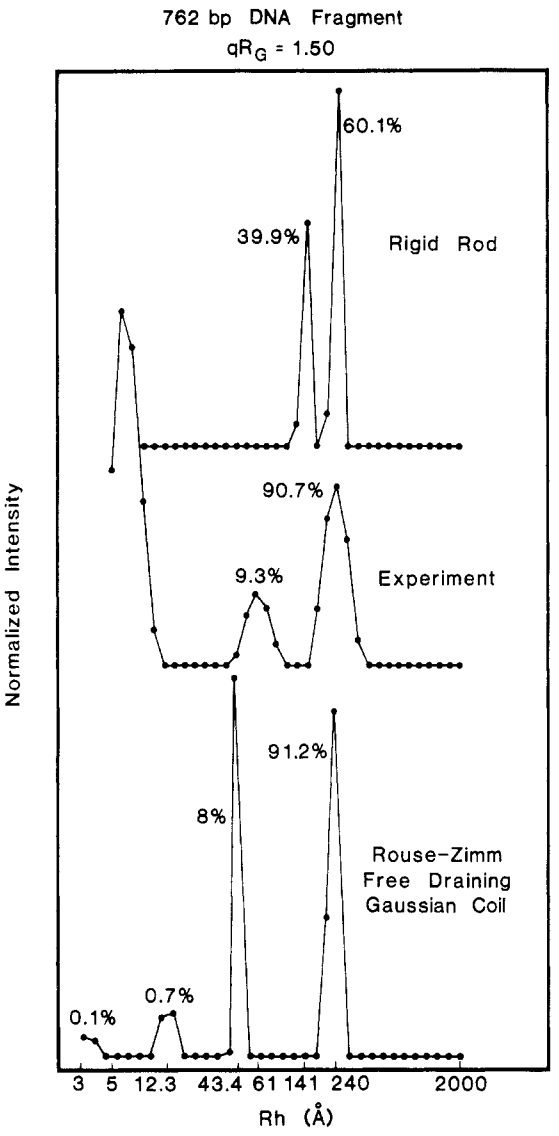

Figure 6. Same as Figure 5 for the 762-bp fragment.

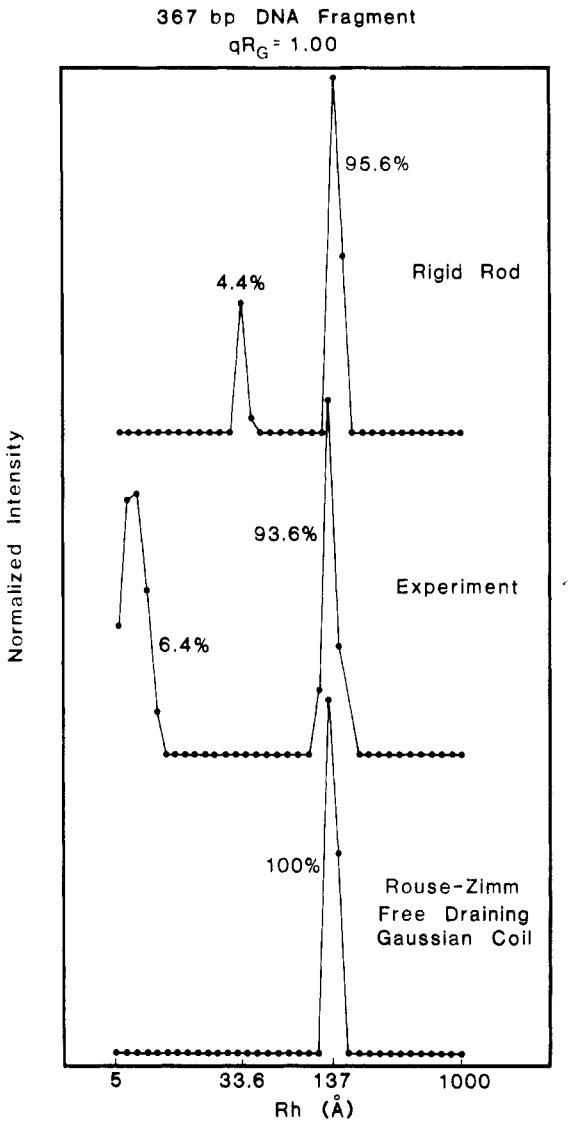

Figure 7. Same as Figure 5 for the 367-bp fragment.

free-draining Rouse–Zimm model. At the experimental angles, a single decay time is predicted by this model. The "size polydispersity" of the experimental peak is 1.005. The same number is obtained from the CONTIN analysis for the Rouse–Zimm model. This suggests that the experimental distribution function is composed of a single decay time. This is not conclusive because the smaller peak for the rigid-rod distribution function has an amplitude of only 4.4%. It is possible that a very small amplitude for a second decay time could be present in the experimental distribution, and only one peak is observed with a small "size polydispersity" due to analytic smoothing. A comparison of the experimental and free-draining Rouse–Zimm distribution functions for the 2311-bp fragment is presented in I.

V. Conclusion

The translational diffusion coefficients for the four DNA restriction fragments are in good agreement with the diffusion coefficients for semistiff chains predicted by Yamakawa and Fujii. The molecular weight dependence of the diffusion coefficient agrees well with that predicted by Yamakawa and Fujii and with the Rouse–Zimm model in the nondraining limit with stiffness added via using R_G from eq 11. The relatively large dependence of the diffusion coefficient on the molecular weight

Table IX
Peak Positions and Their Amplitudes from the Distribution Function: Rod and Coil Limits and Experiment

DNA	peak no.	rod size, Å	rod % amp	coil size, Å	coil % amp	expt size, Å	expt % amp
367	1	336	95.6	137	100	133	93.6
	2	34	4.4			7	6.4
762	1	235	60.1	237	91.2	240	90.7
	2	141	39.9	43	8.0	61	9.3
	3			12	0.7		
	4			4	0.1		
1010	1	300	28.0	300	91.8	300	93.3
	2	210	72.0	54	7.5	65	6.7
	3			5	0.7		

found for the three smaller restriction fragments is a clear manifestation of the effects of chain stiffness.

The value of the first internal/rotational decay time is in very good agreement with the predictions of the Rouse–Zimm model in the free-draining limit, when the radius of gyration from the wormlike coil model and the experimental value of the diffusion coefficient are used. The values of the first internal/rotational decay time are approximately half the values predicted by Yamakawa and Yoshizaki for the 2311–762-bp fragments, and with the values predicted by Hagerman and Zimm for the 1010- and 762-bp fragments. The nondraining Rouse–Zimm model does not predict the experimental values very well.

The first internal/rotational decay times seem to be a more sensitive test of the fit of a model than do the diffusion coefficients since the former depend on the third power of the contour length while the translational diffusion coefficients depend on the inverse first power of the contour length in the rigid-rod limit. These times, however, cannot be measured by DLS with the same high precision as those due to translational diffusion. The experimental distribution functions from CONTIN are in better agreement with the free-draining Rouse–Zimm model than the rigid-rod model. It is very likely that models which incorporate both the appropriate amount of stiffness and hydrodynamic interactions would give data fits similar to those of the free-draining Rouse–Zimm model with experimentally determined diffusion coefficients and radii of gyration.[7]

Acknowledgment. This work was supported by NSF Grant CHE-88-14641 to R.P. and by the NSF MRL program through the Center for Materials Research at Stanford University. We are grateful to Sami Gottlieb for her invaluable assistance in preparing the DNA samples and to Professor Stuart A. Allison for stimulating discussions of Brownian dynamics simulations of DNA fragments.

References and Notes

(1) Lewis, R. J.; Huang, J. H.; Pecora, R. *Macromolecules* **1985**, *18*, 1530.
(2) Provencher, S. W. *Comput. Phys. Commun.* **1982**, *27*, 213, 229.
(3) Provencher, S. W. *CONTIN User's Manual*; Technical Report ENBL-DA02; European Molecular Biology Laboratory: Heidelberg, 1980.
(4) Provencher, S. W. *Makromol. Chem.* **1979**, *180*, 201.
(5) Provencher, S. W.; Hendrix, J.; De Maeyer, L.; Paulussen, N. *J. Chem. Phys.* **1978**, *69*, 4237.
(6) Sorlie, S. S.; Pecora, R. *Macromolecules* **1988**, *21*, 1437.
(7) Allison, S. A.; Sorlie, S. S.; Pecora, R. *Macromolecules*, in press.
(8) Marko, M. A.; Chipperfield, R.; Birnboim, H. C. *Anal. Biochem.* **1982**, *121*, 382.
(9) Lis, J. T.; Schleif, R. *Nucleic Acids Res.* **1975**, *2*, 383.
(10) Wheeler, F. C.; Fishel, R. A.; Warner, R. C. *Anal. Biochem.* **1977**, *73*, 260.
(11) Vogelstein, B.; Gillespie, D. *Proc. Natl. Acad. Sci. U.S.A.* **1979**, *76*, 615.
(12) Ziola, B. R.; Scraba, D. G. *Anal. Biochem.* **1976**, *72*, 366.
(13) Tabak, H. F.; Flavell, R. A. *Nucleic Acids Res.* **1978**, *5*, 2321.
(14) Blin, N.; Gabain, A. V.; Bujard, H. *FEBS Lett.* **1975**, *53*, 84.
(15) Smith, H. O. *Methods Enzymol.* **1980**, *65*, 371.
(16) Maniatis, T.; Fritsch, E. F.; Sambrook, J. *Molecular Cloning, A Laboratory Manuel*; Cold Spring Harbor: New York, 1982.
(17) Maier, K. R. Ph.D. Thesis, Stanford University, Stanford, California, 1986.
(18) Yamakawa, H. *Modern Theory of Polymer Solutions*; Harper and Row: New York, 1971.
(19) Perico, A.; Piaggio, P.; Cuniberti, C. *J. Chem. Phys.* **1975**, *62*, 2690.
(20) Tsunashima, Y.; Hirata, M.; Nemoto, N.; Kajiwara, K.; Kurata, M. *Macromolecules* **1987**, *20*, 2862.
(21) Rey, A.; Freire, J. J.; Garcia de la Torre, J. *J. Chem. Phys.* **1989**, *90*, 2035.
(22) Hagerman, P. J.; Zimm, B. H. *Biopolymers* **1981**, *20*, 1481.
(23) Broersma, S. *J. Chem. Phys.* **1960**, *32*, 1626, 1632; **1981**, *74*, 6989.
(24) Yamakawa, H.; Fujii, M. *J. Chem. Phys.* **1976**, *64*, 5222.
(25) Yoshizaki, T.; Yamakawa, H. *J. Chem. Phys.* **1984**, *81*, 982.
(26) Pecora, R. *J. Chem Phys.* **1964**, *40*, 1604; **1968**, *48*, 4126; **1968**, *49*, 1032.
(27) Zimm, B. H. *J. Chem Phys.* **1956**, *24*, 269.
(28) Lewis, R. J.; Pecora, R. *Macromolecules* **1986**, *19*, 2074.
(29) Lewis, R. J.; Pecora, R.; Eden, D. *Macromolecules* **1986**, *19*, 134.
(30) Berne, B. J.; Pecora, R. *Dynamic Light Scattering*; Wiley-Interscience: New York, 1976.
(31) Hagerman, P. J. *Biopolymers* **1983**, *22*, 811.
(32) Lewis, R. J.; Allison, S. A.; Eden, D.; Pecora, R. *J. Chem. Phys.* **1988**, *89*, 2490.
(33) Lewis, R. J. Ph.D. Thesis, Stanford University, Stanford, California, 1985.
(34) Flory, P. J. *Principles of Polymer Chemistry*; Cornell University Press: Ithaca, NY, 1953.